

## 2.2 W/mm at 94 GHz in AlN/GaN/AlN High-Electron-Mobility Transistors on SiC

Austin Hickman,\* Reet Chaudhuri, Lei Li, Kazuki Nomoto, Neil Moser, Michael Elliott, Matthew Guidry, Keisuke Shinohara, James C. M. Hwang, Huili Grace Xing, and Debdeep Jena

Aluminum nitride (AlN) offers novel potential for electronic integration and performance benefits for high-power, millimeter-wave amplification. Herein, load-pull power performance at 30 and 94 GHz for AlN/GaN/AlN high-electron-mobility transistors (HEMTs) on silicon carbide (SiC) is reported. When tuned for peak power-added efficiency (PAE), the reported AlN/GaN/AlN HEMT shows PAE of 25% and 15%, with associated output power ( $P_{\text{out}}$ ) of 2.5 and 1.7 W mm<sup>-1</sup>, at 30 and 94 GHz, respectively. At 94 GHz, the maximum  $P_{\text{out}}$  generated is 2.2 W mm<sup>-1</sup>, with associated PAE of 13%.

transistors (HEMTs) have dominated output power records at gigahertz (GHz) frequencies, with demonstrations of 40 W mm<sup>-1</sup> at 4 GHz<sup>[1]</sup> via AlGaN/GaN heterostructure, 13.7 W mm<sup>-1</sup> at 30 GHz<sup>[2]</sup> via AlGaN/GaN/InGaN structure, and 8 W mm<sup>-1</sup> at 94 GHz<sup>[3]</sup> via N-polar GaN HEMT. These results have become increasingly relevant for both commercial (5 G and beyond, automotive radar) and defense (SATCOM, radar) applications, all of which are pushing into the mm-wave frequency range (30–300 GHz).

### 1. Introduction

In the pursuit of high-power amplification at gigahertz frequencies, gallium nitride (GaN) has emerged as the premier material platform. While competitive wide-bandgap materials such as silicon carbide (SiC) show comparable high-voltage switching performance, GaN's high electron saturation velocity uniquely positions it for high-voltage, millimeter-wave (mm-wave) applications. Indeed, GaN high-electron-mobility

To further improve upon the advantages offered by GaN HEMTs, our group introduced HEMTs on an aluminum nitride (AlN) buffer layer.<sup>[4–6]</sup> By replacing the AlGaN top barrier with AlN and the typical GaN buffer layer with AlN, the AlN/GaN/AlN heterostructure offers increased thermal conductivity, improved carrier confinement for thin GaN channels (<30 nm), and superior vertical scalability of the top barrier when compared to other conventional top barrier materials such as AlGaN or InAlN. Other groups have also shown promising results from AlN-based devices, including HEMTs on AlN substrates, demonstrating 15 W mm<sup>-1</sup> at X-band<sup>[7]</sup> and AlN buffer breakdown of 5 MV cm<sup>-1</sup>.<sup>[8]</sup> HEMTs using an AlN top barrier have been demonstrated, including the GaN HEMT record  $f_T/f_{\text{max}}$  of 454/444 GHz,<sup>[9–11]</sup> a W-band power amplifier with 27% PAE and associate output power of 1.3 W,<sup>[12]</sup> a K<sub>a</sub>-band low-noise amplifier with a noise figure of less than 2,<sup>[13]</sup> and 4.5 W mm<sup>-1</sup> at 40 GHz,<sup>[14]</sup> all on an AlN/GaN/AlGaN heterostructure. AlN/GaN HEMTs have shown record output power for Ga-polar HEMTs at W-band, with  $P_{\text{out}} = 4$  W mm<sup>-1</sup> at 94 GHz.<sup>[15]</sup> Beyond the radio frequency (RF) HEMT, aluminum nitride offers the potential for monolithic integration of high-current GaN/AlN p-type field effect transistor (pFETs)<sup>[16–18]</sup> and crystalline AlN bulk acoustic wave filters,<sup>[19]</sup> both of which are enabled by the AlN buffer layer. Additional integration is made possible by the SiC substrate in the form of substrate-integrated waveguides (SIWs) and antennas.<sup>[20]</sup> This integrated ecosystem is referred to as the AlN platform, enabling the coexistence of high-power nitride complementary metal oxide semiconductor (CMOS), RF filters, monolithic microwave-integrated circuits (MMICs), and RF waveguides and antenna, all on one monolithic chip.<sup>[21]</sup>

Recently, our group showed large signal response for AlN/GaN/AlN HEMTs at 30 GHz, with 29% peak PAE and associated gain and power of 7 dB and 2.5 W mm<sup>-1</sup>, respectively.<sup>[22]</sup> In this work,

A. Hickman, R. Chaudhuri, L. Li, K. Nomoto, H. G. Xing, D. Jena  
 Electrical and Computer Engineering  
 Cornell University  
 Ithaca, NY 14853, USA  
 E-mail: alh288@cornell.edu


N. Moser, M. Elliott  
 Wright-Patterson Air Force Base  
 Dayton, OH 45433, USA

M. Guidry  
 U.C. Santa Barbara  
 Santa Barbara, CA 93106, USA

K. Shinohara  
 Teledyne Scientific and Imaging  
 Thousand Oaks, CA 91360, USA

J. C. M. Hwang, H. G. Xing, D. Jena  
 Material Science and Engineering  
 Cornell University  
 Ithaca, NY 14853, USA

H. G. Xing, D. Jena  
 Kavli Institute  
 Cornell University  
 Ithaca, NY 14853, USA

 The ORCID identification number(s) for the author(s) of this article can be found under <https://doi.org/10.1002/pssa.202200774>.

DOI: 10.1002/pssa.202200774

measuring devices on the same sample, we demonstrate the first W-band large signal measurements of AlN/GaN/AlN HEMTs, with measured peak output power of  $2.2 \text{ W mm}^{-1}$  at 94 GHz.

## 2. Device Fabrication

The 2 nm GaN cap, 4 nm AlN barrier, 200 nm GaN channel, and 500 nm AlN buffer heterostructure was grown via plasma-assisted molecular beam epitaxy (PAMBE) on 6 H-SiC, as shown in **Figure 1a**. It has been found that the two dimensional electron gas (2DEG) mobility in AlN/GaN/AlN heterostructures increases by increasing the GaN channel layer thickness, increasing from  $\approx 650 \text{ cm}^2 \text{ V}^{-1} \text{ s}$  at 30 nm to  $> 1000 \text{ cm}^2 \text{ V}^{-1} \text{ s}$  at 500 nm. Hence, even though a thin ( $< 30 \text{ nm}$ ) strained GaN channel is desired for maximum backbarrier confinement, the heterostructure used in this work had a 200 nm-thick GaN channel layer as a tradeoff between carrier confinement and mobility. A controlled comparison of the effect of channel layer thickness on the output powers of the RF HEMTs is under way. Partial relaxation of the AlN barrier layer is expected due to 0.6% strain in the 200 nm GaN channel.<sup>[23]</sup> Transport characteristics were measured via Hall effect at room temperature, showing a mobility of  $586 \text{ cm}^2 \text{ V}^{-1} \text{ s}$  and sheet concentration of  $3.2 \times 10^{13} \text{ cm}^{-2}$ . The HEMT processing started with regrown ohmic contacts. The sample was patterned with a Cr/SiO<sub>2</sub> hardmask, and the 2DEG sidewall was exposed with a chlorine (Cl)-based dry etch. Heavily n-type doped ([Si]  $\approx 10^{20} \text{ cm}^{-3}$ ) GaN was regrown in the etched region via PAMBE, establishing ohmic contacts to the 2DEG. After hardmask removal, the HEMTs were isolated via a Cl-based dry etch, and Ti/Au ohmic contacts were deposited on top of the regrown region via e-beam evaporation. A trilayer resist stack and electron beam lithography were used to define the T-gate contacts. The Ni/Au gate metal was also deposited via e-beam evaporation. 100 nm of silicon nitride was then deposited via plasma-enhanced chemical vapor deposition (PECVD) as a passivation layer. The cross-sectional representation and scanning electron microscope (SEM) image of the fully processed AlN/GaN/AlN HEMT are shown in **Figure 1**.

## 3. Results and Remarks

The contact resistance to 2DEG achieved via n++ GaN was  $0.23 \Omega \text{ mm}$ . The AlN/GaN/AlN HEMT highlighted in this report had a gate length of 60 nm. The device showed excellent DC characteristics with on-currents up to  $3 \text{ A mm}^{-1}$ , transconductance ( $g_m$ ) of  $0.68 \text{ S mm}^{-1}$  (**Figure 2a**), and on/off ratio of more than  $10^4$ . The highly scalable top barrier layer, in this case 6 nm thick (4 nm AlN, 2 nm GaN cap), prevents significant short-channel effects for the given gate length of 60 nm. Pulsed  $I_D V_D$  measurements with a pulse width of 500 ns were used to characterize the dispersion of the HEMT. Previous demonstrations of AlN/GaN/AlN HEMTs showed relatively high levels of DC-to-RF dispersion  $> 15\%$ ,<sup>[5,6]</sup> limiting the gain and output power at GHz frequencies. The pulsed  $I_D V_D$  in this report was measured using a 500 ns pulsewidth and 0.05% duty cycle. Prior to large signal measurements, the dispersion of these HEMTs at  $2.5 \text{ A mm}^{-1}$  is  $\approx 5\%$  (**Figure 2c**). The bias-dependent S-parameters were measured in the range of 0.05–40.05 GHz. The system was calibrated using short-open-load-thru structures and de-embedded with on-chip open and short patterns. From the s-parameters, the cutoff frequency ( $f_c$ ) and maximum oscillation frequency ( $f_{\text{max}}$ ) of 124 and 221 GHz are shown in **Figure 2d**.

The large signal characteristics were measured using two Maury microwave passive load-pull system sat 30 and 94 GHz. At both frequencies, the device was biased for class-AB operation at a quiescent drain voltage of 12 V. **Figure 3a** shows the load-pull power sweep for the  $2 \times 25 \mu\text{m}$  AlN/GaN/AlN HEMT at 30 GHz. When tuned for peak efficiency, the device demonstrates a PAE of 25% with associated  $P_{\text{out}}$  of  $2.5 \text{ W mm}^{-1}$  and gain ( $G_T$ ) of 5.9 dB. At 94 GHz, the max PAE of 15% associated  $P_{\text{out}}$  of  $1.7 \text{ W mm}^{-1}$  and gain ( $G_T$ ) of 3.1 dB (**Figure 3b**). At maximum power, the HEMT shows  $2.2 \text{ W mm}^{-1}$  at 94 GHz.

The AlN/GaN/AlN HEMT large signal performance measured in this report was likely limited by the degradation of on-current that occurred during large signal measurement. The lack of surface treatment before SiN passivation may have resulted in a significant amount surface states still remaining after passivation, leading to significant dispersion once the

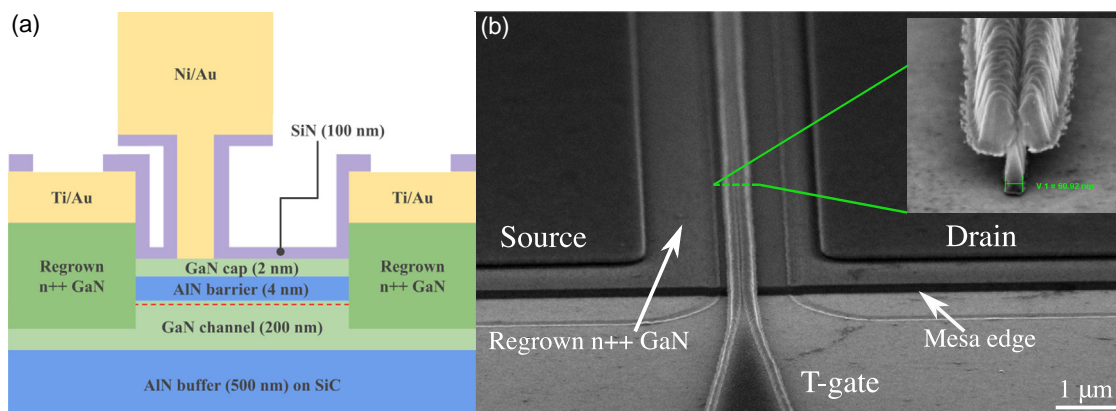


**Figure 1.** a) The cross-sectional representation of the fully processed AlN/GaN/AlN HEMT. b) SEM image of the processed device prior to passivation. One finger of the  $2 \times 25$  micrometer HEMT. The inset image shows a T-gate on the sample with the same exposure conditions as the measured device, demonstrating a gate length of 60 nm.

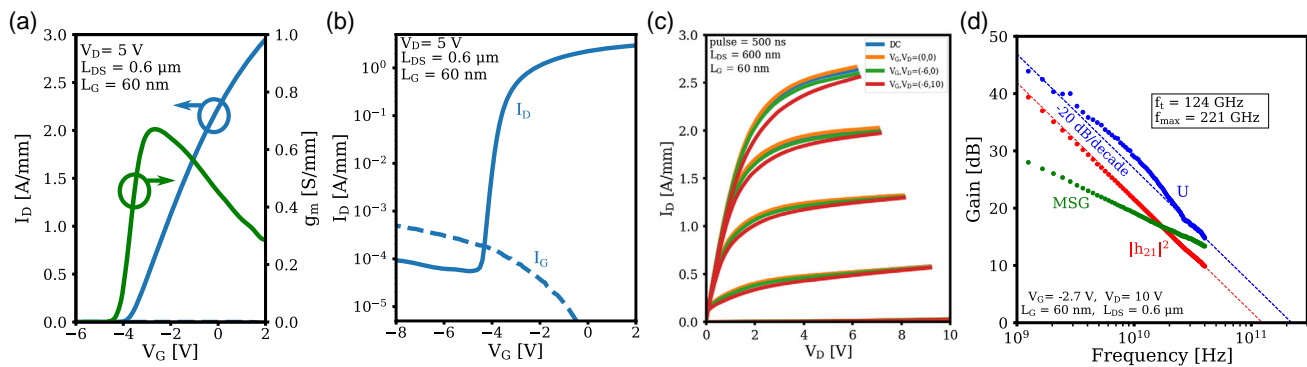


**Figure 2.** a) The linear-scale transfer curve of the AlN/GaN/AlN HEMT demonstrating a transconductance of  $0.68 \text{ S mm}^{-1}$  and threshold voltage of  $-4 \text{ V}$ . b) The log-scale transfer curve showing an on/off ratio  $10^4$ , limited by gate leakage. c) The pulsed  $I_D V_D$  characteristics. Prior to large signal measurements, the dispersion is  $\approx 5\%$ . d) The small-signal characteristics, demonstrating an  $f_t/f_{\max} = 124/221 \text{ GHz}$ , respectively.

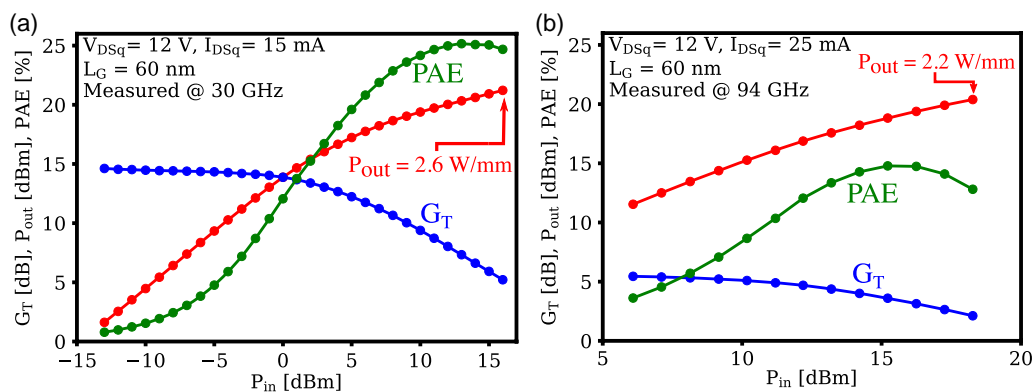


**Figure 3.** a) The power sweep characteristics at 30 GHz. At peak efficiency of 25%, the HEMT shows an output power of  $2.5 \text{ W mm}^{-1}$  and gain of 5.9 dB. At 94 GHz b), the peak efficiency is 15% with associated output power of  $1.7 \text{ W mm}^{-1}$  and gain of 3.1 dB. The maximum observed output power for the device at 30 and 94 GHz is 2.6 and  $2.2 \text{ W mm}^{-1}$ , respectively.

device is stressed under large signal operation. An additional factor could be the thicker GaN channel, which increased the strain in the AlN top barrier, further contributing to device degradation at high biases. Therefore, the next generation of AlN/GaN/AlN HEMTs will feature a thinner GaN channel to reduce stress in the AlN top barrier and increase the back barrier. Additionally, an in situ cleaning step in the PECVD system will be incorporated prior to SiN passivation deposition. This will reduce the number of surface states present and reduce dispersion at GHz frequencies. Long-term efforts aim at in situ passivation of the AlN/GaN/AlN heterostructure.<sup>[23]</sup> Potential MBE-grown passivation materials include crystalline and amorphous AlN, as well as SiN.

## 4. Conclusion

This letter reports the first large signal performance of AlN/GaN/AlN HEMTs at W-band, showing over  $2 \text{ W mm}^{-1}$  at 94 GHz. The most likely limitations in this generation of devices have been identified, and future work is under way to alleviate them. With these improvements, significantly higher output powers for AlN/GaN/AlN HEMTs are anticipated at 30 and 94 GHz.

High output power, combined with novel integration potential, make the AlN platform an attractive candidate for future millimeter-wave electronic systems.

## Acknowledgements

This work was supported by Semiconductor Research Corporation (SRC) Joint University Microelectronics Program (JUMP), AFOSR (FA9550-20-1-0148), and NSF DMR (1710298). This work was performed in part at the Cornell NanoScale Facility, a member of the National Nanotechnology Coordinated Infrastructure, supported by NSF NNCI-2025233, at the Cornell Center for Materials Research, supported by NSF MRSEC DMR-1719875, and at the UCSB HFM Lab (Professors U. K. Mishra and R. A. York), supported by ONR and ARO DURIP grants (including N00014-13-1-0814).

## Conflict of Interest

The authors declare no conflict of interest.

## Data Availability Statement

The data that support the findings of this study are available from the corresponding author upon reasonable request.

## Keywords

AlN, GaN, millimeter waves

Received: November 14, 2022

Revised: January 8, 2023

Published online:

- [1] Y.-F. Wu, M. Moore, A. Saxler, T. Wisleder, P. Parikh, in *Device Research Conf. - Conf. Digest, DRC*, University Park, PA **2006**, pp. 151–152, ISBN 0780397495.
- [2] Y. Wu, M. Moore, A. Abrahamsen, P. Parikh, S. Heikman, A. Burk, in *2007 IEEE Int. Electron Devices Meeting*, IEEE, Piscataway, NJ **2007**, pp. 405–407.
- [3] B. Romanczyk, U. K. Mishra, X. Zheng, M. Guidry, H. Li, N. Hatui, C. Wurm, A. Krishna, E. Ahmadi, S. Keller, *IEEE Electron Device Lett.* **2020**, *41*, 349.
- [4] G. Li, R. Wang, J. Guo, J. Verma, Z. Hu, Y. Yue, F. Faria, Y. Cao, M. Kelly, T. Kosel, H. G. Xing, D. Jena, *IEEE Electron Device Lett.* **2012**, *33*, 661.
- [5] A. Hickman, R. Chaudhuri, S. J. Bader, K. Nomoto, K. Lee, H. G. Xing, S. Member, D. Jena, S. Member, A. In, *IEEE Electron Device Lett.* **2019**, *40*, 1293.
- [6] A. Hickman, R. Chaudhuri, L. Li, K. Nomoto, S. J. Bader, J. C. Hwang, H. G. Xing, D. Jena, *IEEE J. Electron Devices Soc.* **2020**, *9*, 121.
- [7] S. Ozaki, J. Yaita, A. Yamada, Y. Kumazaki, Y. Minoura, T. Ohki, N. Okamoto, N. Nakamura, J. Kotani, *Appl. Phys. Express* **2021**, *14*, 4.
- [8] I. Abid, R. Kabouche, C. Bougerol, J. Pernot, C. Masante, R. Comyn, Y. Cordier, F. Medjdoub, *Micromachines* **2019**, *10*, 10.
- [9] Y. Tang, K. Shinohara, D. Regan, A. Corrión, D. Brown, J. Wong, A. Schmitz, H. Fung, S. Kim, M. Micovic, *IEEE Electron Device Lett.* **2015**, *36*, 549.
- [10] K. Shinohara, A. Corrión, D. Regan, I. Milosavljevic, D. Brown, S. Burnham, P. Willadsen, C. Butler, A. Schmitz, D. Wheeler, A. Fung, M. Micovic, in *2010 Int. Electron Devices Meeting*, IEEE, Piscataway, NJ **2010**, p. 672, ISBN 9781424474196.
- [11] K. Shinohara, D. Regan, A. Corrión, D. Brown, S. Burnham, P. J. Willadsen, M. Cunningham, C. Butler, A. Schmitz, S. Kim, B. Holden, D. Chang, V. Lee, A. Ohoka, P. M. Asbeck, M. Micovic, in *2011 Int. Electron Devices Meeting*, Washington DC, Vol. 2, **2011**, p. D 1.
- [12] A. Margomenos, A. Kurdoghlian, M. Micovic, K. Shinohara, D. F. Brown, A. L. Corrión, H. P. Moyer, S. Burnham, D. C. Regan, R. M. Grabar, C. McGuire, M. D. Wetzel, R. Bowen, P. S. Chen, H. Y. Tai, A. Schmitz, H. Fung, A. Fung, D. H. Chow, in *Technical Digest - IEEE Compound Semiconductor Integrated Circuit Symp., CSIC*, IEEE, Piscataway, NJ **2014**, pp. 14–17.
- [13] M. Micovic, D. Brown, D. Regan, J. Wong, J. Tai, A. Kurdoghlian, F. Herrault, Y. Tang, S. D. Burnham, H. Fung, A. Schmitz, I. Khalaf, D. Santos, E. Prophet, H. Bracamontes, C. McGuire, R. Grabar, in *IEEE Compound Semiconductor Integrated Circuit Symp.*, IEEE, Piscataway, NJ **2016**, pp. 3–6.
- [14] E. Dogmus, R. Kabouche, A. Linge, E. Okada, M. Zegaoui, F. Medjdoub, *Phys. Status Solidi (A)* **2017**, *214*, 8.
- [15] K. Harrouche, R. Kabouche, E. Okada, F. Medjdoub, *IEEE J. Electron Devices Soc.* **2019**, *7*, 1145.
- [16] S. Bader, H. Lee, R. Chaudhuri, S. Huang, A. Hickman, A. Molnar, H. Xing, D. Jena, H. Then, N. Chowdhury, T. Palacios, *IEEE Trans. Electron Devices* **2020**, *67*, 4010.
- [17] R. Chaudhuri, S. J. Bader, Z. Chen, D. A. Muller, H. G. Xing, D. Jena, *Science* **2019**, *365*, 1454.
- [18] K. Nomoto, R. Chaudhuri, S. J. Bader, L. Li, A. Hickman, S. Huang, H. Lee, T. Maeda, H. W. Then, M. Radosavljevic, P. Fischer, A. Molnar, J. C. M. Hwang, H. G. Xing, D. Jena, in *Technical Digest - Int. Electron Devices Meeting, IEDM* San Francisco, CA **2020**, pp. 8.3.1–8.3.4, <https://doi.org/10.1109/IEDM13553.2020.9371994>.
- [19] J. Miller, J. Wright, H. G. Xing, D. Jena, *Phys. Status Solidi (A)* **2020**, *217*, 2.
- [20] M. J. Asadi, L. Li, W. Zhao, K. Nomoto, P. Fay, H. G. Xing, D. Jena, J. C. M. Hwang, in *IEEE MTT-S Int. Microwave Symp. Digest*, IEEE, Piscataway, NJ **2021**, pp. 1–4.
- [21] A. L. Hickman, R. Chaudhuri, S. J. Bader, K. Nomoto, L. Li, J. Hwang, H. G. Xing, D. Jena, *Semicond. Sci. Technol.* **2021**, *36*, 4.
- [22] A. Hickman, R. Chaudhuri, N. Moser, M. Elliott, K. Nomoto, L. Li, J. C. M. Hwang, H. Grace Xing, D. Jena, in *2021 Device Research Conf. (DRC)*, IEEE, Piscataway, NJ **2021**, pp. 1–2, ISBN 9781665412407, ISSN 15483770.
- [23] R. Chaudhuri, A. Hickman, J. Singhal, J. Casamento, H. G. Xing, D. Jena, *Phys. Status Solidi (A)* **2022**, *219*, 4.